Real-time detection of S($^1D_2$) photofragments produced from the $^1B_2(^1\Sigma_u^+)$ state of CS_2 by vacuum ultraviolet photoelectron imaging using 133 nm probe pulses

Takuya Horio, Roman Spesyvtsev,[a)] Yu Furumido, and Toshinori Suzuki[b)]

Department of Chemistry, Graduate School of Science, Kyoto University, Kitashirakawa Oiwake-cho, Sakyo-Ku, Kyoto 606-8502, Japan

Ultrafast photodissociation dynamics from the $^1B_2(^1\Sigma_u^+)$ state of CS_2 are studied by time-resolved photoelectron imaging using the fourth (4ω, 198 nm) and sixth (6ω, 133 nm) harmonics of a femtosecond Ti:sapphire laser. The $^1B_2$ state of CS_2 was prepared with the 4ω pulses, and subsequent dynamics were probed using the 6ω vacuum ultraviolet (VUV) pulses. The VUV pulses enabled real-time detection of S($^1D_2$) photofragments, produced via $CS_2^*(^1B_2(^1\Sigma_u^+)) \rightarrow CS(X\ ^1\Sigma^+) + S(^1D_2)$. The photoionization signal of dissociating $CS_2^*(^1B_2(^1\Sigma_u^+))$ molecules starts to decrease at about 100 fs, while the S($^1D_2$) fragments appear with a finite (ca. 400 fs) delay time after the pump pulse. Also discussed is the configuration interaction of the $^1B_2(^1\Sigma_u^+)$ state based on relative photoionization cross sections to different cationic states.

---

1. Present address: SUPA, Department of Physics, University of Strathclyde, Glasgow, G4 0NG, UK.
2. Author to whom correspondence should be addressed. Electronic mail: suzuki@kuchem.kyoto-u.ac.jp

I. INTRODUCTION

The $^1B_2(^1\Sigma_u^+) \leftarrow S_0(^1\Sigma_g^+)$ photoabsorption spectrum of jet-cooled CS_2 in 192 – 208 nm shows distinct vibrational progressions of the symmetric stretching (ν_1 = 392 cm^{-1}) and bending (ν_2 = 426 cm^{-1}) modes.[1] The photoexcitation into the $^1B_2(^1\Sigma_u^+)$ state is followed by the dissociation reactions of

$$CS_2^*(^1B_2(^1\Sigma_u^+)) \rightarrow CS(X^1\Sigma^+) + S(^3P_J) \qquad (1a)$$

$$\rightarrow CS(X^1\Sigma^+) + S(^1D_2). \qquad (1b)$$

Here we discuss the reaction dynamics of the singlet dissociation channel (1b).

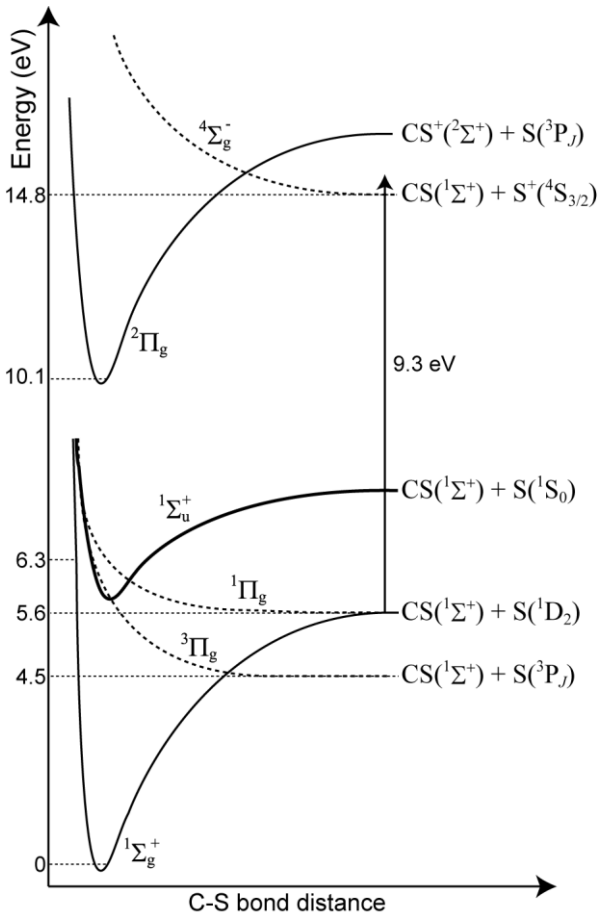

FIG. 1. Schematic potential energy curves of CS_2 in linear geometry. Fine structures in the ground state of atomic sulfur, $^3P_{2,1,0}$, are not shown as their energy differences are less than 0.1 eV.[2]

Figure 1 shows schematic potential energy curves of CS_2 in linear geometry drawn based on the potential energy surfaces (PESs) calculated by time-dependent density functional theory (TDDFT).[3] The potential energy curves of the cationic ground state, $CS_2^+(^2\Pi_g)$ and the excited state, $CS_2^+(^4\Sigma_g^-)$ are also

shown.[4] While the $^1\Sigma_u^+$ is strongly bound, the $^1\Pi_g$ state is repulsive and it creates two a CI along the dissociation coordinate, which mediates the singlet dissociation.

Real-time studies of the photodissociation dynamics from the $^1B_2(^1\Sigma_u^+)$ state have been performed using resonance-enhanced multiphoton ionization (REMPI). Baronavski and Owrutsky[5] and Farmanara et al.[6] employed time-resolved mass spectrometry. Stolow and co-workers[7] employed time-resolved photoelectron spectroscopy (TRPES) to measure the photoelectron kinetic energy distributions (PKEDs) for ionization from dissociating CS_2^* molecules in the $^1B_2$ state. They also extracted molecular-frame photoelectron angular distributions (MF-PADs), which revealed that the electronic character varies from $^1\Sigma_u^+$ to a mixed electronic character of $^1\Sigma_u^+$ + $^1\Pi_g$ within 500 fs time scale.[8] Previously, we have performed time-resolved photoelectron imaging (TRPEI) of this system to measure both PKEDs and laboratory-frame photoelectron angular distributions (LF-PADs) with a time resolution of 20 fs.[9,10] We employed the 7.8-eV vacuum ultraviolet (VUV) probe pulses[10] to observe the vibrational wavepacket motion between the Franck Condon (F.C.) region and the classical turning points for both the ν_1 and ν_2 coordinates. The observed LF-PADs exhibited modulation with an approximately 80 fs period, which is attributed to variation of the electronic character with the ν_1 and ν_2 vibrational motions.

In this study, we revisit this system using sub-17 fs, 9.3-eV VUV probe pulses.[11] As shown in Fig. 1, the 9.3-eV VUV pulses enable single-photon detection of $S(^1D_2)$ photofragments: the energy difference between $S(^1D_2)$ and $S^+(^4S)$, namely the ionization energy of $S(^1D_2)$, is 9.21 eV.[2] We also discuss configuration interaction of the $^1B_2(^1\Sigma_u^+)$ state by measuring partial photoionization cross sections from $^1\Sigma_u^+$ into $X(^2\Pi_g)$, $A(^2\Pi_u)$, and $B(^2\Sigma_u^+)$ states.

II. EXPERIMENTAL METHOD

The experimental setup for DUV-pump and VUV-probe TRPEI has been described in detail.[11-13] Only a brief description is given here. A pulsed molecular beam of CS_2 (~6 %) seeded in helium was generated using an Even-Lavie valve[14] at a stagnation pressure of 0.7 MPa and illuminated by the 4ω pump pulses (198 nm, 6.3 eV) in a stack of acceleration electrodes for velocity-map imaging (VMI[15]). After photoexcitation of CS_2 into the $^1B_2(^1\Sigma_u^+)$ state, time-delayed 6ω pulses (133 nm, 9.3 eV) probed the dissociation dynamics using single-photon ionization. As shown in Fig. 1, while the photodissociation gives rise to two atomic fragments of $S(^3P_J)$ and $S(^1D_2)$, only $S(^1D_2)$ is ionized using 6ω probe pulses.

One modification of our apparatus from our last TRPEI study is the introduction of a piezo-driven mirror mount for a DUV focusing mirror (UV-enhanced aluminum coating, r = −1,000 mm). This has enabled finer adjustment of the spatial overlap between the DUV and VUV pulses on a molecular beam. Two-dimensional (2D) projections of three-dimensional (3D) photoelectron scattering distributions were measured as a function of the delay time with 50 ± 0.1 fs step. The acquisition time for the projection image at each delay time was 13 s, and the measurement was repeated 20 times. The 20 images at each delay time were combined and then analyzed to reconstruct 3D scattering distributions using p-BASEX.[16] A background photoelectron image due to one-color photoionization signals by each pulse (4ω + 4ω and 6ω + 6ω) was subtracted prior to the reconstruction. The total photoelectron yield as a function of the delay time was also measured by monitoring the output current from a microchannel plate (MCP) detector.

In (1 + 1') resonance-enhanced multiphoton ionization with linearly polarized pump and probe pulses with parallel polarizations, the time-dependent photoionization cross-section, $I(E,\theta, t)$, can be expressed as

$$I(E,\theta,t) = \frac{\sigma(E,t)}{4\pi}\left[1+\beta_2(E,t)P_2(\cos\theta)+\beta_4(E,t)P_4(\cos\theta)\right], \qquad (1)$$

where E, θ, and t respectively denote photoelectron kinetic energy (PKE), ejection angle with respect to the polarization, and pump-probe delay. $P_n(x)$ is an nth order Legendre polynomial. $\sigma(E,t)$ corresponds to PKEDs, and the coefficients, $\beta_n(E,t)$, are the nth order photoelectron anisotropy parameters.

Since our VMI setup works as a linear time-of-flight (TOF) mass spectrometer by setting the polarity of the acceleration electrodes to positive, we examined TOF mass spectra observed by the 4ω and 6ω pulses. While single-color two-photon ionization of 4ω (the total photon energy = 12.5 eV) yielded only parent ions (CS_2^+), single-color two-photon ionization by 6ω pulses (the total photon energy = 18.6 eV) generated fragment ions of S^+ and CS^+ in addition to CS_2^+. These fragment ions are ascribed to dissociative ionization of CS_2^+; the appearance energies of the fragment ions, S^+ and CS^+, were reported to be 14.81 and 16.16 eV, respectively.[17] At very high gain of MCP detector, small S_2^+ signal was also identified.

III. RESULTS AND DISCUSSION

A. Photoionization signal of S($^1D_2$)

Figure 2 shows the total photoelectron signal measured as a function of the pump-probe delay time. It is noted that a non-vanishing plateau persists even after 2 ps, which has not been seen in previous studies.[3,5-10] This is the ionization signal of the S($^1D_2$) photofragments as explained below.

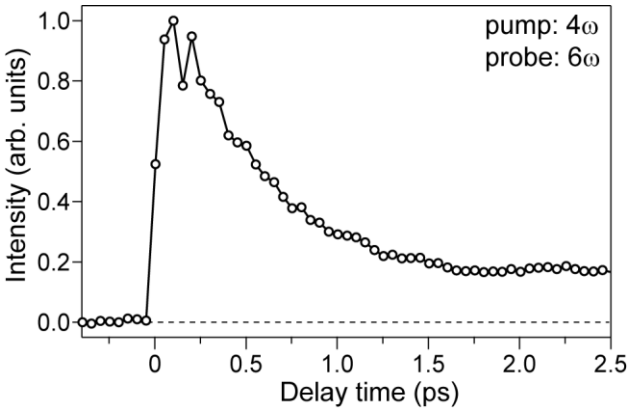

FIG. 2. Photoelectron total yield as a function of the delay time between 4ω (198 nm) and 6ω (133 nm) pulses.

Figures 3(a)-(h) show representative 2D slice images calculated from the velocity-map photoelectron images measured at 49.3, 149.4, 249.5, 399.6, 599.7, 1000.0, 1500.3, and 1900.6 fs, respectively. Comparison of Figs. 2 and 3 reveals that the plateau in the ionization signal corresponds to sharp rings (see Fig. 3(h)). Figure 4(a) shows the PKED extracted from the photoelectron image in Fig. 3(h). Three peaks are observed at 0.19, 0.26, and 0.32 eV.

Yang et al.[18] measured the photoionization efficiency (PIE) spectrum of S($^1D_2$) using a tunable nanosecond VUV laser in the energy range from 9.09 to 10.53 eV, and they observed 35 autoionizing states while negligible direct photoionization. In Fig. 4(b) is shown schematically a part of their PIE spectrum as a function of the excitation energy. All autoionizing states in this energy region have $3s^2 3p^3(^2D^\circ)3d$ configuration, except for the one at 9.53 eV, which has $3s^2 3p^3(^2D^\circ)5s$ configuration. Our broadband 6ω VUV pulse (dashed line) is resonant to these autoionizing states, S^{**}, which decay into $S^+(^4S) + e^-$ continuum in ps time scale.[18] Note that only the $S^+(^4S_{3/2})$ state is created in this energy region as the second ionization limit, $S^+(^2D_{3/2})$, is 11.06 eV higher in energy than S($^1D_2$).[2] The top horizontal axis in Fig. 4(b) indicates the excess energy above the $S^+(^4S_{3/2})$ threshold. Comparison of Fig. 4(a) and (b) reveals that the observed electron kinetic energies in Fig. 4(a) agree very well with the energies expected for autoionization from the states at 9.40, 9.47, and 9.53 eV in Fig. 4(b). Thus the long-lived

photoionization signal is unambiguously assigned to S($^1D_2$), a product of the singlet dissociation channel (1b).

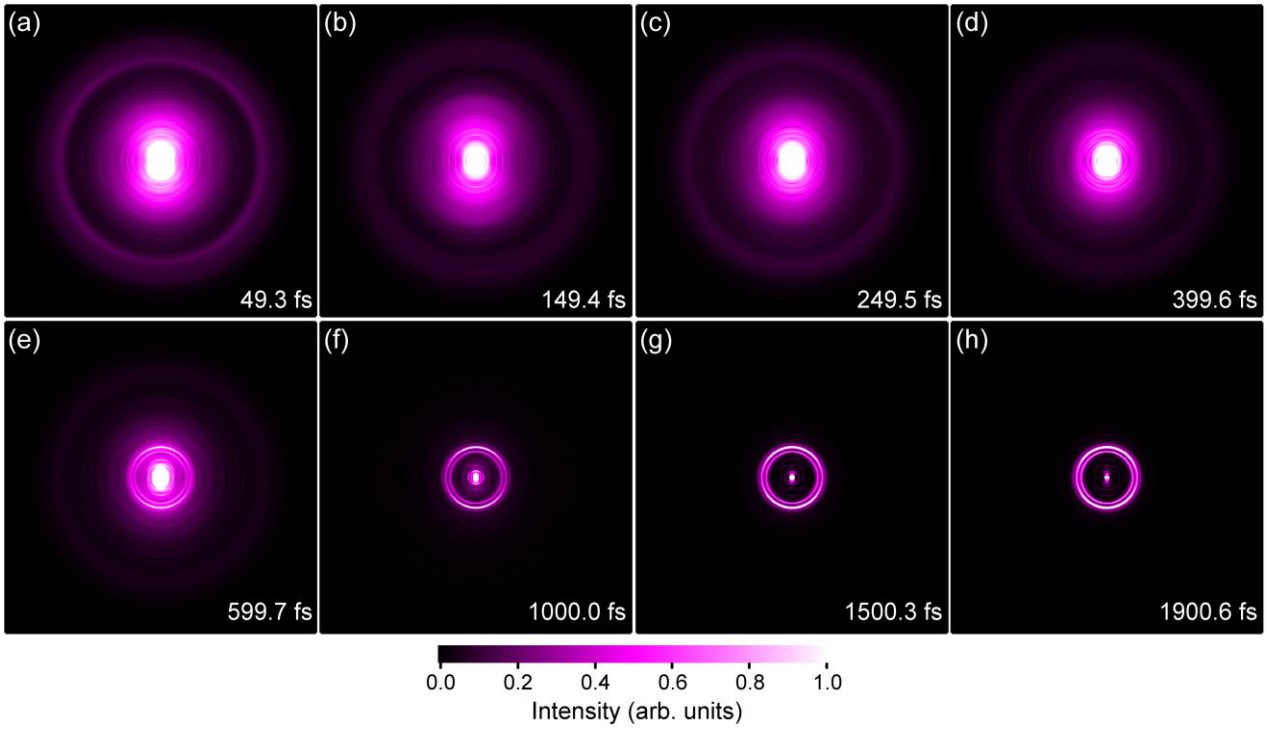

FIG. 3. 2D slices of the 3D photoelectron scattering distributions obtained at the delay times of (a) 49.3, (b) 149.4, (c) 249.5, (d) 399.6, (e) 599.7, (f) 1000.0, (g) 1500.3, and (h) 1900.6 fs. The intensity scale for the images (f), (g), and (h) has been adjusted so that the maximum value is 2.0.

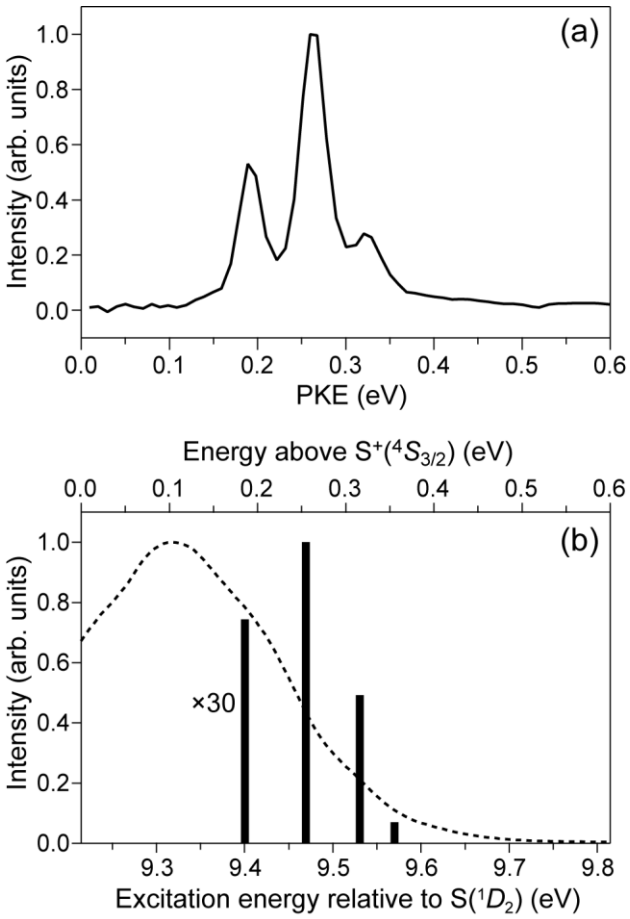

FIG. 4. (a) PKED obtained at 1900.6 fs. (b) Schematic PIE spectrum of S($^1D_2$) (sticks)[18] overlaid with the spectrum of 6ω pulse employed in this study (dashed line).

B. Appearance time of S($^1D_2$)

Close examination of the observed photoelectron images in Figs. 3 reveals that the bright rings from S($^1D_2$) fragments become discernible in 599.7 fs (see Fig. 3(e)). To investigate this in a more quantitative manner, we have constructed a 2D time-energy map of PKEDs extracted from the observed images. Figure 5 shows the PKE region from 0 to 2.0 eV. While the sharp peaks gradually rise with the delay time, their early-time behavior is obscured by an overlapping broad spectrum appearing across the entire PKE region (0 – 2.0 eV). Thus, we first analyzed the decaying component using a signal integrated from 0.50 to 0.54 eV where no atomic signal occurs. To express the decaying signal, the following formula was employed:

$$I(t) = \left[A\exp\left(-\frac{t}{\tau_A}\right) + B\exp\left(-\frac{t}{\tau_B}\right)\right] \otimes g(t) \ , \qquad (2)$$

where $g(t)$ is the cross-correlation function (Gaussian with FWHM of 17 fs)[11] between 4ω and 6ω pulses. As shown in Fig. 6(a), an exponential function with a negative amplitude ($B < 0$ in eq. (2)) was required to phenomenologically describe the early-time "non-exponential" behavior with a lag time prior to population decay, which is consistent with our previous study using 3ω[9] and 5ω[10] probe pulses. Eq. (2) well describes the observed transient signals. The time constants, τ_A and τ_B, determined by the fitting were 598 ± 21 and 93 ± 23 fs, respectively.

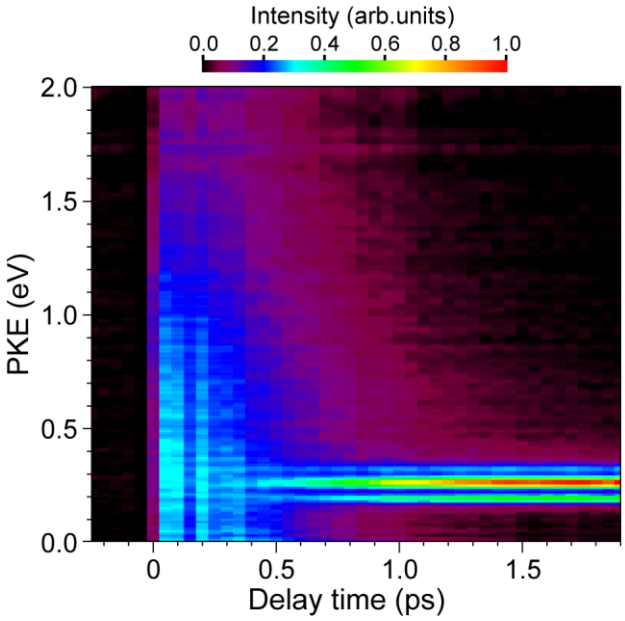

FIG. 5. 2D map of the time-dependent PKEDs from 0 to 2.0 eV extracted from the observed photoelectron images.

For least-squares fitting to the time profile integrated for the selected energy range of 0.15 – 0.35 eV, where the sharp atomic signals occur, the following formula was employed:

$$I(t) = \left[A\exp\left(-\frac{t}{\tau_A}\right) + B\exp\left(-\frac{t}{\tau_B}\right) + C\left\{1-\exp\left(-\frac{t-t_d}{\tau_C}\right)\right\}\right] \otimes g(t) \ , \qquad (3)$$

where t_d is an induction time for the S($^1D_2$) formation. The values of τ_A and τ_B are assumed to be the same as determined by the least-square fittings to the 0.50 – 0.54 eV time profile. The result is presented in Fig. 6(b). As seen in the figure, delayed appearance of S($^1D_2$) photofragments is quite clear. We confirmed that least-squares fitting without t_d entirely fails to reproduce depression observed around 400 fs. From the least square fitting, the time delay, t_d, and time constant, τ_c, for the production of S($^1D_2$) were determined to be 389 ± 26 and 875 ± 121 fs, respectively. We have also measured a time profile of

S^+ ion produced by 4ω-pump and 6ω-probe pulses; however, the "decaying" signal of S^+ due to dissociative ionization of CS_2, $CS_2^+ \rightarrow CS + S^+$, was so large in the observed time profile for S^+ that the delayed appearance of the $S(^1D_2)$ photofragments could not be identified in the S^+ signal. Wang et al.[19] performed *ab initio* multiple spawning simulations for this system and predicted that some dissociation into the $CS(X^1\Sigma^+) + S(^1D_2)$ channel occurs in 70 fs, while delayed appearance has not been discussed in their study.

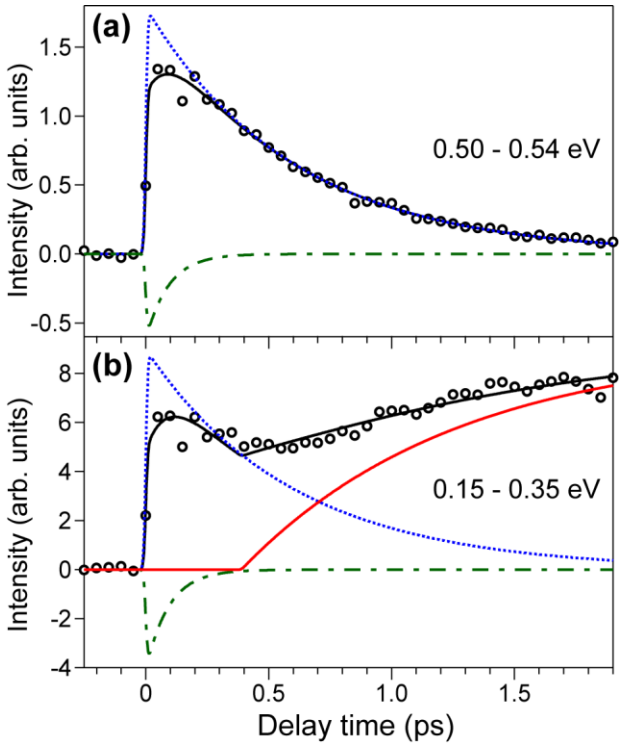

FIG. 6. Photoelectron time profiles for the PKE subsections: (a) 0.50 – 0.54 and (b) 0.15 – 0.35 eV extracted from the 2D map shown in Fig. 5. The results of the least squares fittings are shown with black solid lines. Blue dotted and green dash-dotted lines respectively correspond to the first and second exponential decay functions defined in eq. (2). The time-dependent population of $S(^1D_2)$ photofragments is shown with a red solid line.

Brouard et al.[20] demonstrated that the reaction dynamics of the singlet dissociation channel (1b) is different between above and below the barrier to linearly on the $^1B_2(^1\Sigma_u^+)$ PES; the minimum of the $^1B_2$ state[21,22] and the barrier height[23] have been reported as 46248.7 and 3400 cm^{-1}, respectively. For photoexcitation above the barrier to linearity, Brouard et al. observed an inverted $CS(X^1\Sigma^+)$ vibrational distribution, consistent with many other studies on the 193-nm photolysis (51700 cm^{-1}) of CS_2.[24-30] On the other hand, for photoexcitation below the barrier they found that $CS(X^1\Sigma^+)$ product state distributions are consistent with a statistical energy partitioning and proposed that dissociation below the

barrier occurs primarily on a PES with a deep potential well and without an exit barrier, which is most likely the ground-state PES. The energy of our 4ω pulse is 50505 cm^{-1}, which is about 1000 cm^{-1} above the barrier to linearity.

Close examination of the decaying signal, namely [$CS_2^*(t)$], shown in Fig. 6(a) reveals that [$CS_2^*(t)$] starts to decrease at ca. 100 fs and decays with τ_A (598 fs), while the S($^1D_2$) signal starts to appear at ca. 400 fs (t_d) as shown in Fig. 6(b). These results indicate that photoionization cross section increases within the first 100 fs owing to the change of the electronic character of the ionized $^1B_2$ state, while population decay starts at least at ca. 100 fs. Since the vibrational period of the anti-symmetric stretch (ν_3 = 1567 cm^{-1})[31] is quite short (21 fs), if this population decay is due to dissociation, the S($^1D_2$) signal should appear correspondingly. However, there is a finite time delay, 300 fs, for the initial appearance of the S($^1D_2$) signal in the asymptotic region after the population decay. This indicates that the fragments are not produced directly from the initially prepared $^1B_2$ state, and the wave packet launched in the F. C. region are trapped elsewhere with smaller ionization cross section than from the $^1B_2$ with 6ω VUV probe pulses.

C. Configuration interaction of the $^1B_2(^1\Sigma_u^+)$ state

In this study, we examined PKED at 0 fs to investigate the configuration interaction of the $^1\Sigma_u^+$ excited state of CS_2. The electronic configuration of CS_2 in the ground state ($^1\Sigma_g^+$) is given by

$$[\text{Core orbitals}](5\sigma_g)^2(4\sigma_u)^2(6\sigma_g)^2(5\sigma_u)^2(2\pi_u)^4(2\pi_g)^4(3\pi_u)^0(7\sigma_g)^0(8\sigma_g)^0(6\sigma_u)^0(4\pi_u)^0\cdots. \qquad (4)$$

Figure 7 shows PKED obtained at 0 fs, in which three bands are discernable near 1.0, 2.7, and 5.4 eV in PKE. The point group of the molecule at 0 fs is considered as $D_{\infty h}$. Adiabatic ionization energies for the valence cationic states of CS_2^+, $X(^2\Pi_g)$, $A(^2\Pi_u)$, $B(^2\Sigma_u^+)$, and $C(^2\Sigma_g^+)$, have been measured to be 10.080, 12.698, 14.477, and 16.190 eV, respectively.[32] Since the total photon energy (4ω + 6ω) in the present study is 15.6 eV, $X(^2\Pi_g)$, $A(^2\Pi_u)$, and $B(^2\Sigma_u^+)$ cationic states can be created energetically. Multireference configuration interaction (MRCI) calculation for CS_2^+ by Hochlaf[4] has shown that $X(^2\Pi_g)$, $A(^2\Pi_u)$, and $B(^2\Sigma_u^+)$ cationic states are well described as a single electronic configuration of $(2\pi_g)^{-1}$, $(2\pi_u)^{-1}$, and $(5\sigma_u)^{-1}$, respectively, where $(\phi)^{-1}$ denotes a hole in the ϕ orbital. The maximum PKE values, E_X, E_A, and E_B for each ionic state are indicated with vertical dotted lines in Fig. 7.

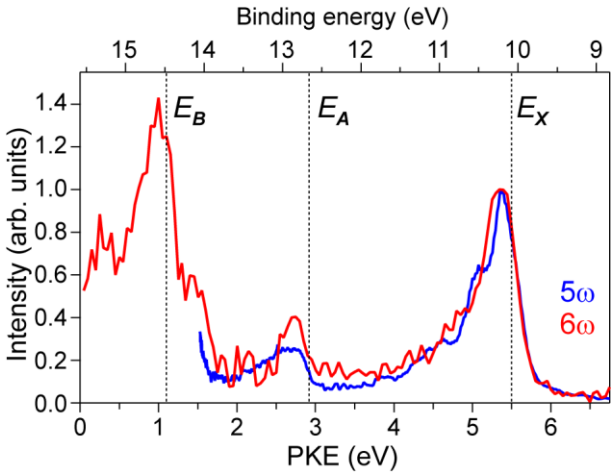

FIG. 7. PKED obtained at 0 fs (red). PKED obtained at 0 fs in our previous study using 5ω probe pulses[10] is also shown (blue). E_X, E_A, and E_B respectively denotes the largest possible PKEs for photoionization into $X(^2\Pi_g)$, $A(^2\Pi_u)$, and $B(^2\Sigma_u^+)$ states.

As seen in Fig. 7, the observed three bands are assigned as photoionization signals from the $^1\Sigma_u^+$ state into $X(^2\Pi_g)$, $A(^2\Pi_u)$, and $B(^2\Sigma_u^+)$ states in descending order of PKE. Since the 6ω spectrum is rather broad (0.3 eV in full width at half maximum) as shown with a dashed line in Fig. 4(b), E_X, E_A, and E_B were calculated for the peak energy (9.32 eV) of the 6ω spectrum. The spectra of $X(^2\Pi_g)$ and $A(^2\Pi_u)$ bands are fully consistent between the present study and our 5ω-probe study[10], and relative photoionization cross sections between $X(^2\Pi_g) \leftarrow {}^1\Sigma_u^+$ and $A(^2\Pi_u) \leftarrow {}^1\Sigma_u^+$ are similar for the 5ω to 6ω probe pulses. The partial photoionization cross sections for $X(^2\Pi_g)$ and $B(^2\Sigma_u^+) \leftarrow {}^1\Sigma_u^+$ are much greater than that for $A(^2\Pi_u) \leftarrow {}^1\Sigma_u^+$, suggesting that the $X(^2\Pi_g)$ and $B(^2\Sigma_u^+)$ cationic states have Koopmans' correlations with electronic configurations of $^1\Sigma_u^+$.

According to VUV photoabsorption spectrum and TDDFT studies of CS_2 by Sunanda et al.[33], the $^1\Sigma_u^+$ electronic excited state created by our 4ω pulses can be denoted as S_3 and has main electronic configurations of $(2\pi_g)^3(3\pi_u)^1$, which is schematically shown in Fig. 8. For simplicity, only one of the degenerate configurations is shown here. Photoionization from $S_3(^1\Sigma_u^+)$ by 6ω VUV pulses occurs into $X(^2\Pi_g)$ due to Koopmans' correlation. Sunanda et al.[33] predicted minor contribution of $(2\pi_g)^3(4\pi_u)^1$ to the $S_3(^1\Sigma_u^+)$ wave function; however the $(2\pi_g)^3(4\pi_u)^1$ configuration does not mediate ionization to $B(^2\Sigma_u^+)$. A possible candidate for the counterpart of configuration interactions to enable ionization to $B(^2\Sigma_u^+)$ is $(5\sigma_u)^1(7\sigma_g)^1$, which has been observed as an intense peak at 11.10 eV in the VUV

photoabsorption spectrum.[33] This electronic state, $S_n(^1\Sigma_u^+)$, is assigned as 4*s* member of the Rydberg series converging to $B(^2\Sigma_u^+)$, and thus has Koopmans' correlation with $B(^2\Sigma_u^+)$, as schematically shown in Fig. 8.

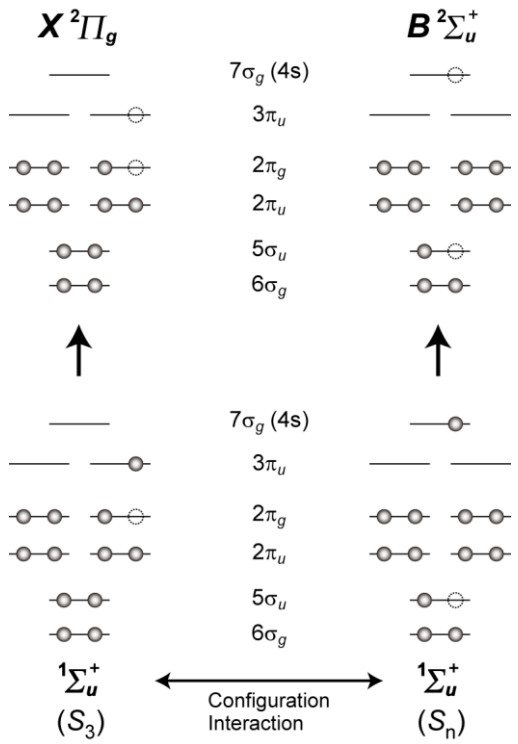

FIG. 8. Electronic configurations for neutral excited and cationic states of CS_2.

Since the $7\sigma_g$ orbital has 4*s* character,[33] one expects that *p* outgoing waves dominate owing to the propensity rule of $\Delta l = +1$, where *l* is an orbital angular momentum in the one-center approximation. Thus, we anticipate relatively high β_2 values for this ionization process.[34] Figure 9 shows the 2D slice image of the photoelectron scattering distribution measured at 0 fs. The directions of the polarization vectors of both 4ω and 6ω pulses are vertical in the plane of the image. It is clear from Fig. 9 that photoelectrons for the $B(^2\Sigma_u^+)$ band are ejected almost parallel to the polarization vectors. The β_2 and β_4 values for the $B(^2\Sigma_u^+)$ band in eq. (1) were found to be 1.2 and 0.3, respectively, while both the β_2 and β_4 values for the $X(^2\Pi_g)$ band were close to zero. The high β_2 value for the $B(^2\Sigma_u^+)$ band is consistent with the expectation.

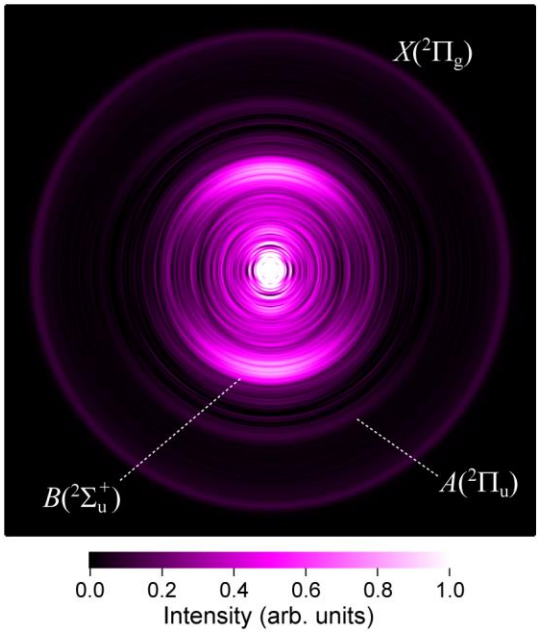

FIG. 9. 2D slice of the 3D photoelectron scattering distributions obtained at 0 fs.

IV. CONCLUSION

We employed TRPEI using 9.3-eV probe pulses to revisit ultrafast photodissociation dynamics from the $^1B_2(^1\Sigma_u^+)$ state (S_3) of CS_2. The 9.3-eV VUV pulses enabled real-time detection of $S(^1D_2)$ photofragments produced from the singlet dissociation channel, $CS_2^*(^1B_2(^1\Sigma_u^+)) \rightarrow CS(X\ ^1\Sigma^+) + S(^1D_2)$. Careful analysis of the rising $S(^1D_2)$ photoionization signal revealed that the $S(^1D_2)$ fragments appear with a finite (ca. 400 fs) delay time after the photoexcitation into the $^1B_2(^1\Sigma_u^+)$ state by the 6.3-eV pulses. The PKED observed at 0 fs reveals large contribution of photoionization processes of $X(^2\Pi_g) \leftarrow S_3(^1\Sigma_u^+)$ and $B(^2\Sigma_u^+) \leftarrow S_3(^1\Sigma_u^+)$.

ACKNOWLEDGMENTS

This work was supported by JSPS KAKENHI Grant Numbers 15H05753 and 15K05388. The authors thank Dr. Y.-I. Suzuki for helpful discussions.

References

[1]R. J. Hemley, D. G. Leopold, J. L. Roebber, and V. Vaida, J. Chem. Phys. **79**, 5219 (1983).

[2]W. C. Martin, R. Zalubas, and A. Musgrove, J. Phys. Chem. Ref. Data **19**, 821 (1990).

[3]C. Z. Bisgaard, O. J. Clarkin, G. R. Wu, A. M. D. Lee, O. Gessner, C. C. Hayden, and A. Stolow, Science **323**, 1464 (2009).

[4]M. Hochlaf, J. Phys. B-at. Mol. Opt. **37**, 595 (2004).

[5]A. P. Baronavski and J. C. Owrutsky, Chem. Phys. Lett. **221**, 419 (1994).

[6]P. Farmanara, V. Stert, and W. Radloff, J. Chem. Phys. **111**, 5338 (1999).

[7]D. Townsend, H. Satzger, T. Ejdrup, A. M. D. Lee, H. Stapelfeldt, and A. Stolow, J. Chem. Phys. **125**, 234302 (2006).

[8]P. Hockett, C. Z. Bisgaard, O. J. Clarkin, and A. Stolow, Nat. Phys. **7**, 612 (2011).

[9]T. Fuji, Y. I. Suzuki, T. Horio, and T. Suzuki, Chem-Asian. J. **6**, 3028 (2011).

[10]R. Spesyvtsev, T. Horio, Y. I. Suzuki, and T. Suzuki, J. Chem. Phys. **142**, 074308 (2015).

[11]T. Horio, R. Spesyvtsev, and T. Suzuki, Opt. Lett. **39**, 6021 (2014).

[12]T. Horio, R. Spesyvtsev, and T. Suzuki, Opt. Express **21**, 22423 (2013).

[13]T. Horio, R. Spesyvtsev, K. Nagashima, R. A. Ingle, Y. Suzuki, and T. Suzuki, J. Chem. Phys. **145**, 044306 (2016).

[14]U. Even, J. Jortner, D. Noy, N. Lavie, and C. Cossart-Magos, J. Chem. Phys. **112**, 8068 (2000).

[15]A. T. J. B. Eppink and D. H. Parker, Rev. Sci. Instrum. **68**, 3477 (1997).

[16]G. A. Garcia, L. Nahon, and I. Powis, Rev. Sci. Instrum. **75**, 4989 (2004).

[17]V. H. Dibeler and J. A. Walker, J. Opt. Soc. Am. **57**, 1007 (1967).

[18]X. L. Yang, J. G. Zhou, B. Jones, C. Y. Ng, and W. M. Jackson, J. Chem. Phys. **128**, 084303 (2008).

[19]K. H. Wang, V. McKoy, P. Hockett, and M. S. Schuurman, Phys. Rev. Lett. **112**, 113007 (2014).

[20]M. Brouard, E. K. Campbell, R. Cireasa, A. J. Johnsen, and W. H. Yuen, J. Chem. Phys. **136**, 044310 (2012).

[21]A. E. Douglas and I. Zanon, Can. J. Phys. **42**, 627 (1964).

[22]A. S. Beatty, R. C. Shiell, D. Chang, and J. W. Hepburn, J. Chem. Phys. **110**, 8476 (1999).

[23]M. F. Arendt and L. J. Butler, J. Chem. Phys. **109**, 7835 (1998).

[24]S. C. Yang, A. Freedman, M. Kawasaki, and R. Bersohn, J. Chem. Phys. **72**, 4058 (1980).

[25]J. E. Butler, W. S. Drozdoski, and J. R. Mcdonald, Chem. Phys. **50**, 413 (1980).

[26]V. R. Mccrary, R. Lu, D. Zakheim, J. A. Russell, J. B. Halpern, and W. M. Jackson, J. Chem. Phys. **83**, 3481 (1985).

[27]I. M. Waller and J. W. Hepburn, J. Chem. Phys. **87**, 3261 (1987).

[28]W. B. Tzeng, H. M. Yin, W. Y. Leung, J. Y. Luo, S. Nourbakhsh, G. D. Flesch, and C. Y. Ng, J. Chem. Phys. **88**, 1658 (1988).

[29]W. S. McGivern, O. Sorkhabi, A. H. Rizvi, A. G. Suits, and S. W. North, J. Chem. Phys. **112**, 5301 (2000).

[30]T. N. Kitsopoulos, C. R. Gebhardt, and T. P. Rakitzis, J. Chem. Phys. **115**, 9727 (2001).

[31]D. J. Donaldson, J. Chem. Phys. **91**, 7455 (1989).

[32]L. S. Wang, J. E. Reutt, Y. T. Lee, and D. A. Shirley, J. Electron. Spectrosc. Relat. Phenom. **47**, 167 (1988).

[33]K. Sunanda, A. Shastri, A. K. Das, and B. N. R. Sekhar, J. Quant. Spectrosc. Ra. **151**, 76 (2015).

[34]R. Spesyvtsev, T. Horio, Y. I. Suzuki, and T. Suzuki, J. Chem. Phys. **143**, 014302 (2015).